Progress In Electromagnetics Research C, Vol. 122, 229–241, 2022

Numerical Analysis of Resonant Characteristics of Graphene Rectangular Microstrip Patch Antenna with Roof Top Functions

Chouaib Chettah[1, *] and Ouarda Barkat[2, 3]

Abstract—In this paper, an analytical model is presented to investigate the resonant characteristics of a graphene rectangular microstrip patch antenna. To take into account the graphene film patch in the full-wave spectral domain technique, surface complex impedance is considered. This impedance is determined by using Kubo formula. A set of roof top sub-domain basis functions are employed to model the current density distribution on the graphene rectangular microstrip patch. The simulation results demonstrate that the designed structure can provide excellent tunable properties in Terahertz frequency region by varying different chemical potentials and relaxation times of graphene film. Variations of dimension of rectangular patch on the resonant frequency and bandwidth of a graphene rectangular microstrip antenna are presented. Finally, numerical results for the dielectric substrates effects on the operating frequencies are also presented. The analysis is validated by comparing the results with a specific example in the literature.

1. INTRODUCTION

Nowadays, wireless communication systems have received enormous interest worldwide in recent decade [1–3]. Rectangular microstrip patch antennas (GRMPAs) have been very popular because of their use in various wireless applications due to their small size, light weight, miniaturized size, wide bandwidth, high efficiency, and low cost [4–6]. They are currently designed to operate at higher frequencies, often at the terahertz (THz) spectrum, to increase the throughput of wireless links with features of low latency and improving the system performance. Researchers have explored the use of graphene for a reconfigurable antenna operating at terahertz frequencies [7–11]. Graphene is attracting great scientific interest thanks to its exceptional electrical and mechanical properties. It is a two-dimensional material formed from a single layer of carbon atoms arranged in a honeycomb crystal lattice. In addition, graphene has very high electrical conductivity thanks to the ballistic transport of electrons. Indeed, electrons move in graphene at a speed that can reach 200 times more than its speed in silicon at room temperature. In particular, these materials make it possible to design nano-antennas up to 100 times more miniature than the smallest current antennas [12–15]. These antennas have the particularity of transmitting data at very high speeds (several hundred gigabits per second) over distances of a few millimeters with low energy consumption. These new antennas could be exploited to improve the communication between various components. Let us quote the example of transfer of the data between the microprocessor and the memory in the smartphones or in the computers. They could still be used as communication devices with wireless nano-sensors, as in the case of RFID systems [16–19]. Recently, there have been a number of investigations of resonant frequencies of GRMPAs. These investigations are based on CST and HFSS computer aided design tools for determining the tunable frequencies [20–25]. However, the

Received 27 June 2022, Accepted 28 July 2022, Scheduled 12 August 2022

* Corresponding author: Chouaib Chettah (chettah_chouaib@yahoo.fr).

[1] Department of Petrochemical, University of 20 August 1955, Skikda, Algeria. [2] Department of Electronics, University of Mentouri Brothers Constantine 1, Algeria. [3] Electromagnetism and Telecommunications Laboratory, University of Mentouri Brothers Constantine 1, Algeria.

accuracy of these approximate models is limited and only suitable for analyzing simple, regularly shaped antenna or thin substrates. Full-wave spectral method is extensively used in microstrip analysis and design. This method gives better results than approximate techniques [26, 27]. In the current paper, we have developed an analytical model for the analysis of GRMPA which has been published little. In the spectral method, the roof top sub-domain basis functions are introduced to expand the unknown current on the GRMPA. The boundary condition for the electric field was used to derive an integral equation for the electric current. Compared to the exiting antenna design, the numerical results, obtained from the implementation of our calculations, have shown the improvement of the bandwidth of graphene rectangular microstrip GRMPA.

2. MATHEMATICAL FORMULATION

Figure 1 shows the geometry of the GRMPA, and the rectangular patch dimensions are the length Lp and width Wp. A rectangular microstrip is printed on a dielectric substrate of thickness d characterized by a permittivity ε_r, and the permeability will be taken as μ_0.

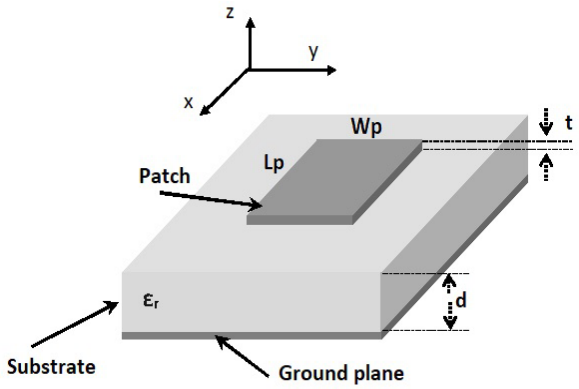

Figure 1. Geometry of graphene rectangular microstrip on uniaxial substrate.

In order to find the dyadic Green's function of the structure, the calculus of transverse field components in the two layer is the first step to start. We will suppose a space time dependence of all the components of the kind $e^{i(\vec{k}\cdot\vec{r}-wt)}$.

The full-wave moment method has been applied extensively and is now a standard approach for analysis of microstrip geometry. In the spectral domainthe transverse field components in the two layer can be obtained using the Fourier transform formulation [28].

$$\tilde{\bar{E}}\left(k_s,z\right) = \iint_{-\infty}^{+\infty} \bar{E}(x,y,z)e^{-i(k_x\cdot x+k_y\cdot y)}dxdy \tag{1}$$

$$\tilde{\bar{H}}\left(k_s,z\right) = \iint_{-\infty}^{+\infty} \bar{H}(x,y,z)e^{-i(k_x\cdot x+k_y\cdot y)}dxdy \tag{2}$$

Starting from Maxwell's equations in the Fourier transform domain and by using the boundary conditions and condition of continuity of E and H fields, after some simple algebraic manipulation, we can find that the relationship between the patch current and the electric field on the patch is given by [29]:

$$\tilde{\bar{E}}\left(k_s\right) = \bar{G}\left(k_s\right)\cdot\tilde{\bar{J}}\left(k_s\right) \tag{3}$$

where $\tilde{\bar{J}}(k_s)$ is the current on the patch, and $\bar{G}(k_s)$ is the spectral dyadic Green's function, whose expression is given by:

$$\bar{G}\left(k_s\right) = \begin{bmatrix} G_{xx} & G_{xy} \\ G_{yx} & G_{yy} \end{bmatrix} = \frac{1}{k_s^2}\begin{bmatrix} k_x & k_y \\ k_y & -k_x \end{bmatrix}\bar{Q}\begin{bmatrix} k_x & k_y \\ k_y & -k_x \end{bmatrix} \tag{4}$$

where

$\vec{k_s}$ is the transverse wave vector given by $\vec{k_s} = k_x \cdot \vec{x} + k_y \cdot \vec{y}$;

k_x and k_y are the wave numbers corresponding to x and y directions, respectively.

Q is given by:

$$\bar{Q} = \begin{bmatrix} Q_{xx} & 0 \\ 0 & Q_{yy} \end{bmatrix} \tag{5}$$

Q_{xx} and Q_{yy} are determined by:

$$Q_{xx} = \frac{k_z}{i\omega\varepsilon_0} \cdot \frac{k_r}{D^e} \cdot \sin(k_r \cdot d) \tag{6}$$

$$Q_{yy} = \frac{1}{i\omega\varepsilon_0} \cdot \frac{k_z^2}{D^h} \cdot \sin(k_r \cdot d) \tag{7}$$

where

$D^e = \varepsilon_r \cdot k_z \cdot \cos(k_r^2 \cdot d) + ik_r \cdot \sin(k_r^2 \cdot d)$;

$D^h = k_r \cdot \cos(k_r^2 \cdot d) + ik_z \cdot \sin(k_r^2 \cdot d)$;

$k_r^2 = \varepsilon_r k_0^2 - k_s^2, k_0^2 = \omega^2 \varepsilon_0 \mu_0$;

$k_z^2 = k_0^2 - k_s^2$.

The surface current $\bar{J}(r_s)$ on the patch can be expanded into a series of known basis functions $J_{xn}(r_s)$ and $J_{ym}(r_s)$.

$$\bar{J}(r_s) = \sum_{n=1}^{N} a_n \begin{bmatrix} J_{xn}(r_s) \\ 0 \end{bmatrix} + \sum_{m=1}^{M} b_m \begin{bmatrix} 0 \\ J_{ym}(r_s) \end{bmatrix} \tag{8}$$

where a_n and b_m are the unknown coefficients to be determined in the x and y directions, respectively. The main problem is how to select the basis functions associated with the complete orthogonal set of TM and TE modes of rectangular microstrip antenna. It is prudent to assume basis functions which approximate the actual current distributions. The current density J is modeled as a summation of piecewise linear subdomain basis functions known as rooftop basis functions. These functions are characterized by their triangular shape along the direction of current flow and rectangular cross section in the orthogonal direction, mathematically; the sub-domain basis functions for the components of the current are described as [30]:

$$J_x(r_s) = \sum_{m=1}^{M} \sum_{n=1}^{N+1} I_x^{mn} \bigwedge_m(x) \coprod_n(y) \tag{9}$$

$$J_y(r_s) = \sum_{m=1}^{N+1} \sum_{n=1}^{N} I_y^{mn} \bigwedge_n(y) \coprod_m(x) \tag{10}$$

where the functions $\bigwedge$ and $\coprod$ are "triangle" and "pulse" functions, respectively. The current density functions for the spectral domain can be written as:

$$\tilde{J}_x(k_s) = \sum_{m=1}^{M} \sum_{n=1}^{N+1} I_x^{mn} F_x^{mn}(k_s) \tag{11}$$

$$\tilde{J}_y(k_s) = \sum_{m=1}^{M} \sum_{n=1}^{N+1} I_y^{mn} F_y^{mn}(k_s) \tag{12}$$

where

$$F_x^{mn}(k_s) = \Delta x \Delta y \left[\frac{\sin\left(\frac{k_y \Delta y}{2}\right)}{\frac{k_y \Delta y}{2}} \right] \left[\frac{\sin\left(\frac{k_x \Delta x}{2}\right)}{\frac{k_x \Delta x}{2}} \right]^2 e^{\left(-ik_x x_m - ik_y y_n + \frac{ik_y \Delta y}{2}\right)} \tag{13}$$

$$F_y^{mn}(k_s) = \Delta x \Delta y \left[\frac{\sin\left(\frac{k_x \Delta x}{2}\right)}{\frac{k_x \Delta x}{2}}\right]\left[\frac{\sin\left(\frac{k_y \Delta y}{2}\right)}{\frac{k_y \Delta y}{2}}\right]^2 e^{\left(-ik_x x_m - ik_y y_n + \frac{ik_x \Delta x}{2}\right)} \tag{14}$$

To include the effect of the graphene of the microstrip antenna in full-wave analysis, the conductivity is determined by using Kubo formula. Graphene is modeled as a sheet conductor whose surface conductivity consists of two terms, intraband conductivity and interband conductivity. However, in the Terahertz-frequency band, the first term dominates the value of total conductivity whereas the second term has no significant effect on the overall surface conductivity within this band. Hence, the conductivity of graphene can be expressed by using only intraband term, which can be evaluated as [31–33]:

$$\sigma(\omega) = \sigma_{intra}(\omega) + \sigma_{\text{inter}}(\omega) \tag{15}$$

where

$$\sigma_{\text{intra}}(\omega) = \frac{2q_e^2 K_b T i}{\pi\hbar^2(\omega + i\tau^{-1})} \ln\left(2\cosh\left(\frac{\mu_c}{2K_b T}\right)\right) \tag{16}$$

$$\sigma_{\text{inter}}(\omega) = \frac{q_e^2}{4\pi\hbar} \ln\left(\frac{2|\mu_c| - (\omega - i\tau^{-1})\hbar}{2|\mu_c| + (\omega - i\tau^{-1})\hbar}\right) \tag{17}$$

where K_b is the Boltzmann constant, $\hbar$ the reduced Planck's constant, q_e the electron charge, ω the angular frequency, τ the relaxation time, T the temperature, and μ_c the chemical potential.

$$Z_s = \frac{1}{\sigma} \tag{18}$$

Z_s: is the equivalent surface impedance of the graphene;

σ: frequency dependent surface conductivity computed using Eq. (16).

The integral equation for the currents on the graphene rectangular microstrips is then formulated using the dyadic Green's function and forcing the tangential electric field to vanish on the patch.

$$\bar{E}(r_s) = \frac{1}{(2\pi)^2} \int dk_s F(k_s, r_s)\left(\bar{G}(k_s) - \bar{Z}_s\right)\tilde{J}(k_s) = 0 \tag{19}$$

where

$$\bar{Z}_S = \begin{vmatrix} Z_S & 0 \\ 0 & Z_S \end{vmatrix}$$

Substituting Eq. (5) into Eq. (20) and using the selected basis functions as testing functions, we obtain the following homogeneous matrix equation:

$$\begin{bmatrix} \left(\bar{B}_{kn}\right)_{N\times N} & \left(\bar{B}_{km}\right)_{N\times M} \\ \left(\bar{B}_{ln}\right)_{M\times N} & \left(\bar{B}_{lm}\right)_{M\times M} \end{bmatrix} \cdot \begin{bmatrix} (a_n)_{N\times 1} \\ (b_m)_{M\times 1} \end{bmatrix} = 0 \tag{20}$$

where

$$\bar{B}_{kn} = \iint_{-\infty}^{+\infty} dk_s \frac{1}{k_s^2}\left(G_{xx} - Z_s\right)\tilde{J}_{xk}(-k_s)\tilde{J}_{xn}(k_s) \tag{21}$$

$$\bar{B}_{km} = \iint_{-\infty}^{+\infty} dk_s \frac{k_x k_y}{k_s^2} G_{xy}\tilde{J}_{xk}(-k_s)\tilde{J}_{ym}(k_s) \tag{22}$$

$$\bar{B}_{ln} = \iint_{-\infty}^{+\infty} dk_s \frac{k_x k_y}{k_s^2} G_{yx}\tilde{J}_{yl}(-k_s)\tilde{J}_{xn}(k_s) \tag{23}$$

$$\bar{B}_{lm} = \iint_{-\infty}^{+\infty} dk_s \frac{1}{k_s^2}\left(G_{yy} - Z_s\right)\cdot\tilde{J}_{yl}(-k_s)\cdot\tilde{J}_{ym}(k_s) \tag{24}$$

Therefore, for the existence of nontrivial solutions, the determinant of Eq. (21) must be zero.

$$\det(\bar{B}(f)) = 0 \tag{25}$$

In general, the root of Eq. (26) is the characteristic equation for the complex resonant frequency.

$$f = fr + i * fi \tag{26}$$

where

fr: is the resonant frequency;

$fr/2 \cdot fi$: is the quality factor Q of the antenna.

3. RESULTS AND DISCUSSION

In order to observe the effect of conductivity of the graphene $\sigma(\omega)$ on frequency behavior, we have simulated, in Fig. 2, the real and imaginary parts of the total conductivity of the graphene, according to Eq. (15) as a function of the frequency, for several different chemical potentials μ_c (0.1 to 0.4 eV).

The calculated $\sigma(\omega)$, as shown in Fig. 2(a), is found in low frequency range, and the differences of real part of graphene conductivity among the four cases of μ_c are significant. At higher frequencies $f \geq 1.8$ THz, the imaginary part of graphene conductivity becomes significant and must be considered. From the results of Fig. 2(b), it can be seen that the effect of varying the frequency on the real part of $\sigma(\omega)$ is significant only for values below the frequency 2 THz.

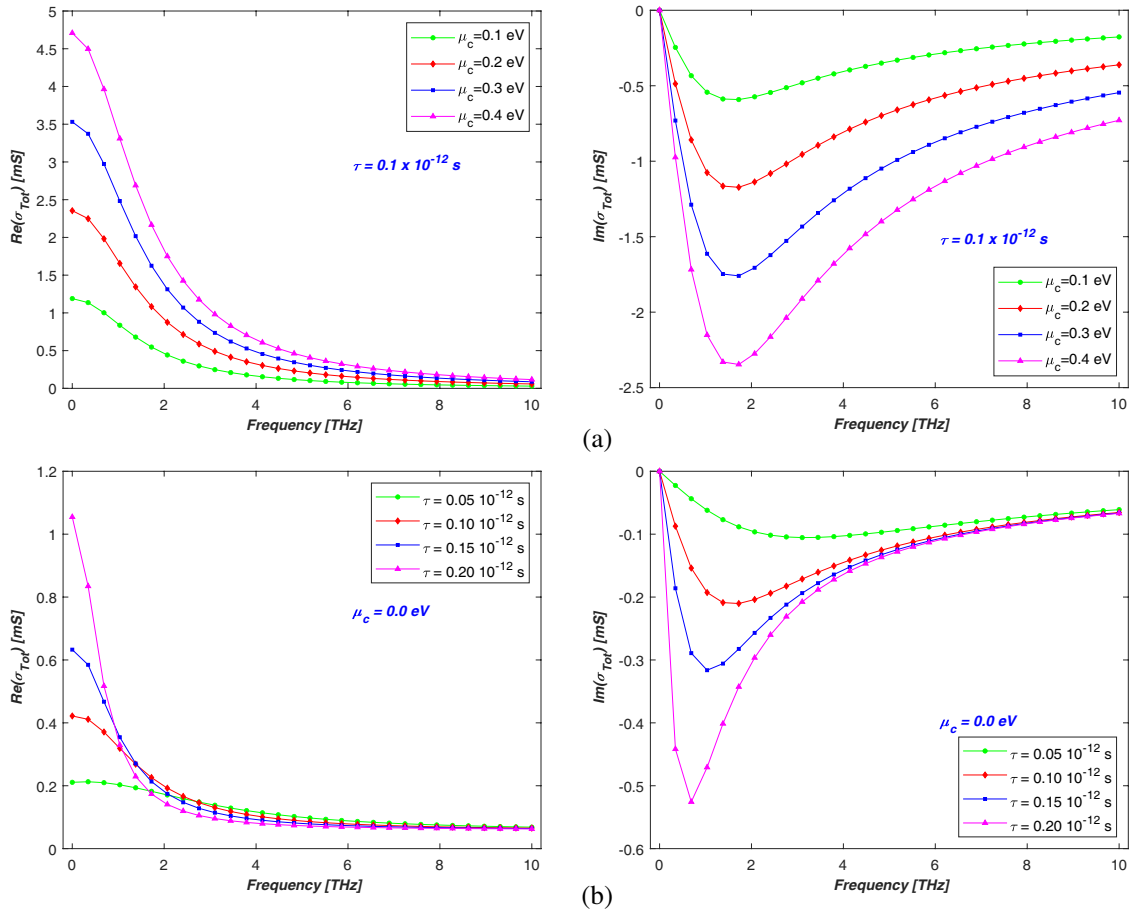

Figure 2. Real and Imaginary parts of total graphene conductivity at room temperature ($T = 300$ K) for different values of: (a) Chemical potential μ_c with $\tau = 0.1 \times 10^{-12}$ s, (b) Relaxation time τ with $\mu_c = 0.0$ eV.

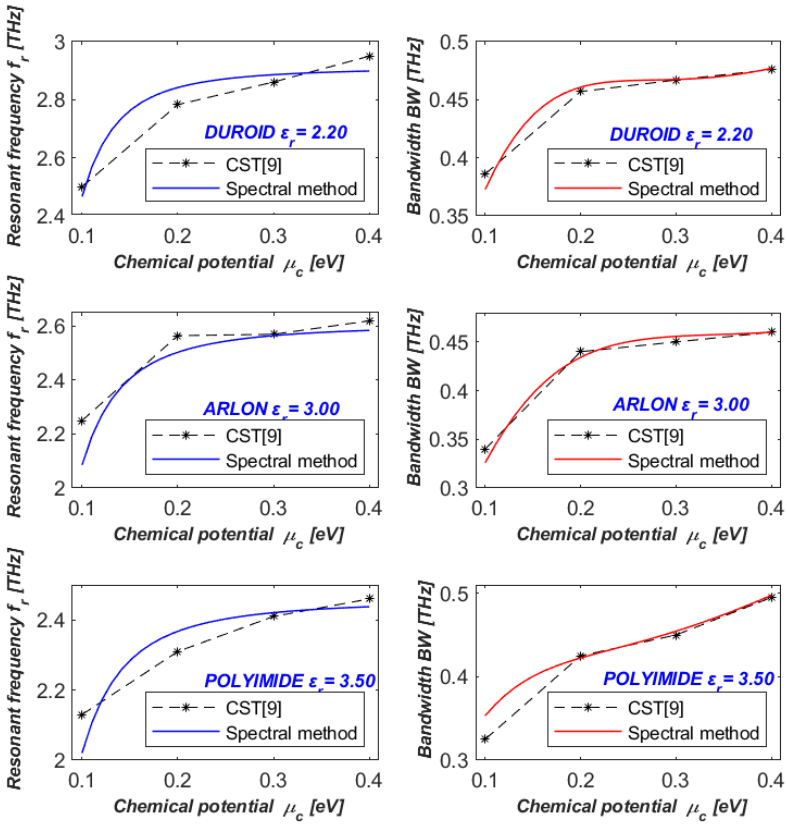

Figure 3. The graphs that compare the resonant frequencies (FR) and bandwidth (BW) obtained through the spectral method and previously published results.

The aim in this section is to validate our results, and the codes have been developed with the MATLAB language. In order to validate our results, we have proceeded to a comparison with cases presented in the literature. In Fig. 3 and Table 1, we have calculated the resonant frequencies (fr) and bandwidth (BW) of GRMPA structure with a single layer for the mode TM_{01}, for different values of chemical potential (μ_c) and (ε_r). The considered structure was modeled by using the spectral method. The comparison of fr and BW was conducted for three different values of relative permittivity (ε_r), which have been suggested in [9] Table 1. Note that the agreement is very good. It is observed from Fig. 3 that in order to enhance the bandwidth of the GRMPA structure, the chemical potential value must be adjusted. Thus it can be concluded that the effect of chemical potential (μ_c) on the resonant frequency and bandwidth of a GRMPA structure cannot be ignored and must be taken into account in the design stage.

In this section, typical numerical results, for the resonant frequency (fr) and bandwidth (BW) of some examples of GRMPA structure, are presented and analyzed.

3.1. Effect of Relaxation Time (τ)

Figure 4 shows the influence of the relaxation time (τ) and chemical potential (μ_c) on the variation of the resonance frequency and the bandwidth, for a patch of rectangular shape with dimensions ($Wp = 28.79\,\mu$m, $Lp = 23.33\,\mu$m, $t = 4.7\,$nm).

The graphene patch is printed on a substrate (DUROID) of permittivity $\varepsilon_r = 2.20$ and thickness $d = 3\,\mu$m. It is clear from Table 2 and Fig. 4 that the resonance frequency increases rapidly until the chemical potential (μ_c) reaches the value 0.35 eV. After this value, the increase in the resonance frequency becomes less important. Bandwidth results are also presented. We note that the bandwidth increases with increasing chemical potential and the relaxation time (τ). A good agreement was found

Table 1. Comparison of simulated and calculated resonant frequencies and bandwidth of rectangular Microstrip Patch Antenna, with $Wp = 28.79\,\mu m$, $Lp = 23.33\,\mu m$ and $\varepsilon_r = (2.20, 3.00, 3.50)$.

		Simulation CST [9]	Spectral method	Simulation CST [9]	Spectral method
	μ_c [eV]	FR [THz]	FR [THz]	BW [THz]	BW [THz]
DUROID $\varepsilon_r = 2.20$	0.1	2.500	2.466	0.386	0.373
	0.2	2.783	2.842	0.457	0.461
	0.3	2.861	2.886	0.467	0.467
	0.4	2.950	2.899	0.476	0.477
ARLON $\varepsilon_r = 3.00$	0.1	2.250	2.085	0.340	0.326
	0.2	2.565	2.504	0.440	0.434
	0.3	2.570	2.565	0.450	0.455
	0.4	2.620	2.584	0.460	0.459
POLYIMIDE $\varepsilon_r = 3.50$	0.1	2.130	2.020	0.325	0.353
	0.2	2.310	2.368	0.425	0.422
	0.3	2.410	2.421	0.450	0.455
	0.4	2.460	2.438	0.495	0.498

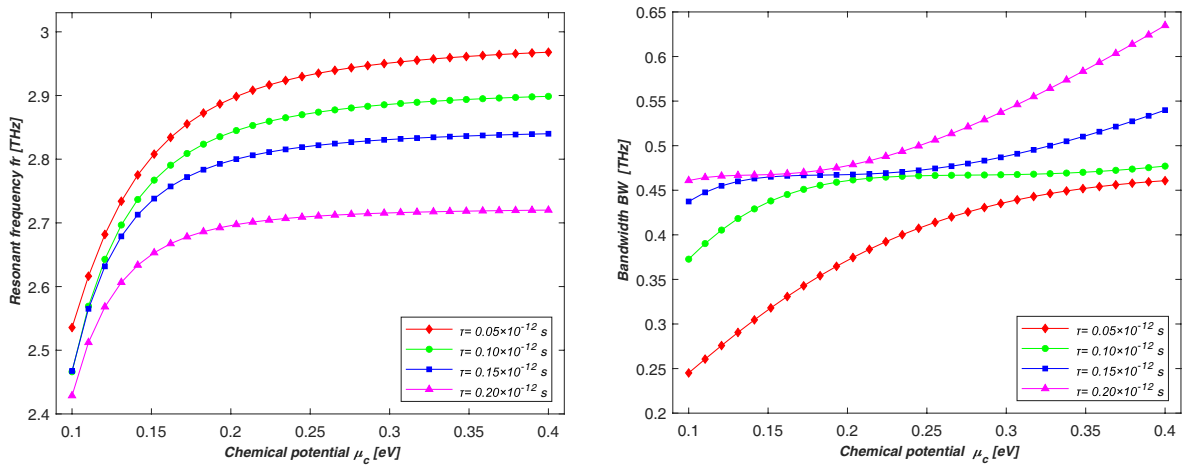

(a) (b)

Figure 4. Resonant frequency and bandwidth versus chemical potential for different values of relaxation time.

between our results and those of [9]. On the other hand, the resonance frequency decreases when the relaxation time increases.

3.2. Effect of Dielectric Constant of Substrate (ε_r)

In this subsection, the effects of dielectric constant of substrate (ε_r) on the resonant frequency and the bandwidth are determined as function of chemical potential (μ_c) for different values of dielectric constant ($\varepsilon_r = 2.10$, 2.20, 3.00, and 3.38) of a GRMPA structure with dimensions $Wp = 28.79\,\mu m$, $Lp = 23.33\,\mu m$, and $d = 3\,\mu m$. It is evident from Table 3 and Fig. 5 that the resonant frequency and bandwidth of (GRMPA) structure decrease with the increase of ε_r. In addition, there is an improvement in bandwidth

Table 2. Resonant frequency and bandwidth versus chemical potential for different values of relaxation time.

	μ_c [eV]	$\tau = 0.05$ ps	$\tau = 0.10$ ps	$\tau = 0.15$ ps	$\tau = 0.20$ ps
FR [THz]	0.1	2.536	2.467	2.467	2.428
	0.2	2.895	2.842	2.798	2.696
	0.3	2.951	2.886	2.831	2.716
	0.4	2.968	2.899	2.839	2.720
BW [THz]	0.1	0.245	0.373	0.437	0.461
	0.2	0.371	0.461	0.468	0.477
	0.3	0.436	0.467	0.488	0.540
	0.4	0.461	0.477	0.539	0.635

Table 3. Resonant frequency and bandwidth versus chemical potential for different values of dielectric constant of substrate.

	μ_c [eV]	TEFLON ($\varepsilon_r = 2.10$)	DUROID ($\varepsilon_r = 2.2$)	ROGER RO 3003 ($\varepsilon_r = 3.00$)	ROGER RO 4003C ($\varepsilon_r = 3.38$)
FR [THz]	0.1	2.637	2.466	2.085	2.202
	0.2	3.071	2.842	2.503	2.368
	0.3	3.132	2.886	2.565	2.421
	0.4	3.151	2.899	2.584	2.438
BW [THz]	0.1	0.381	0.373	0.326	0.330
	0.2	0.491	0.461	0.434	0.398
	0.3	0.506	0.467	0.455	0.427
	0.4	0.512	0.477	0.459	0.464

as chemical potential (μ_c) increases. These behaviors agree with those discovered theoretically obtained by the electromagnetic field simulation software CST for resonant frequency and bandwidth of GRMPA structure [8, 9].

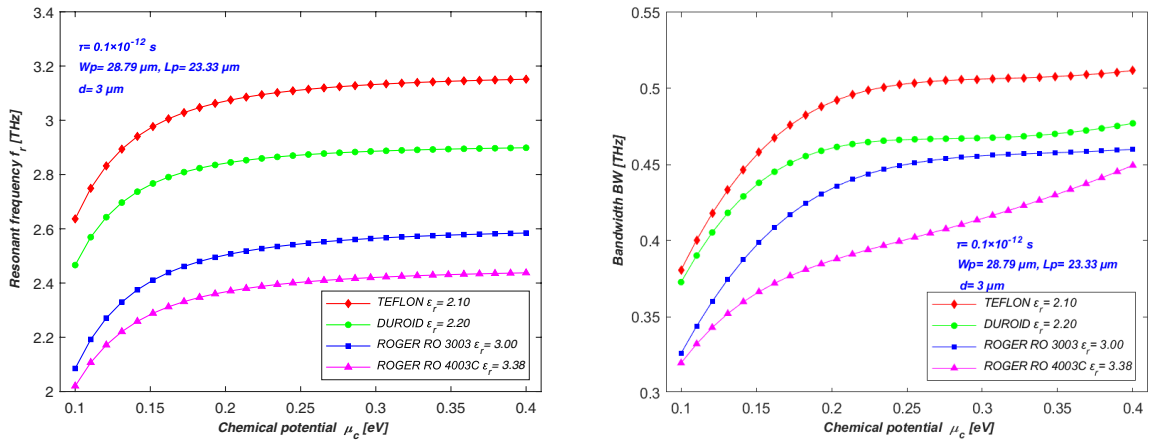

(a) (b)

Figure 5. Resonant frequency and bandwidth versus chemical potential for different values of dielectric constant of substrate.

3.3. Effect of Width of patch (Wp)

In Figure 6 and Table 4, effects of width of patch rectangular (Wp) on the resonant frequencies and the bandwidth have been calculated for various chemical potentials. This can be obtained by having length $Lp = 23.33\,\mu\text{m}$, dielectric substrate of thickness ($d = 3\,\mu\text{m}$) fabricated using DUROID ($\varepsilon_r = 2.20$), and the relaxation time of conductivity of Graphene is $\tau = 10^{-13}\,\text{s}$. The resonant frequencies and the bandwidth of GRMPA structure for the fundamental mode TM_{01} are computed by the present approach. It is clear from these results that the resonance frequency and bandwidth increase when the chemical potential (μ_c) increases and are stable at μ_c higher than 0.3 eV, but they are decreased when the width of patch increases.

Table 4. Resonant frequency and bandwidth versus chemical potential for different values of width of patch.

	μ_c [eV]	$Wp = 20\,\mu\text{m}$	$Wp = 30\,\mu\text{m}$	$Wp = 40\,\mu\text{m}$	$Wp = 50\,\mu\text{m}$
FR [THz]	0.1	2.405	2.245	2.063	1.957
	0.2	3.054	2.619	2.297	2.141
	0.3	3.113	2.660	2.327	2.166
	0.4	3.127	2.671	2.336	2.173
BW [THz]	0.1	0.373	0.334	0.267	0.255
	0.2	0.483	0.449	0.386	0.343
	0.3	0.499	0.475	0.432	0.361
	0.4	0.505	0.480	0.446	0.365

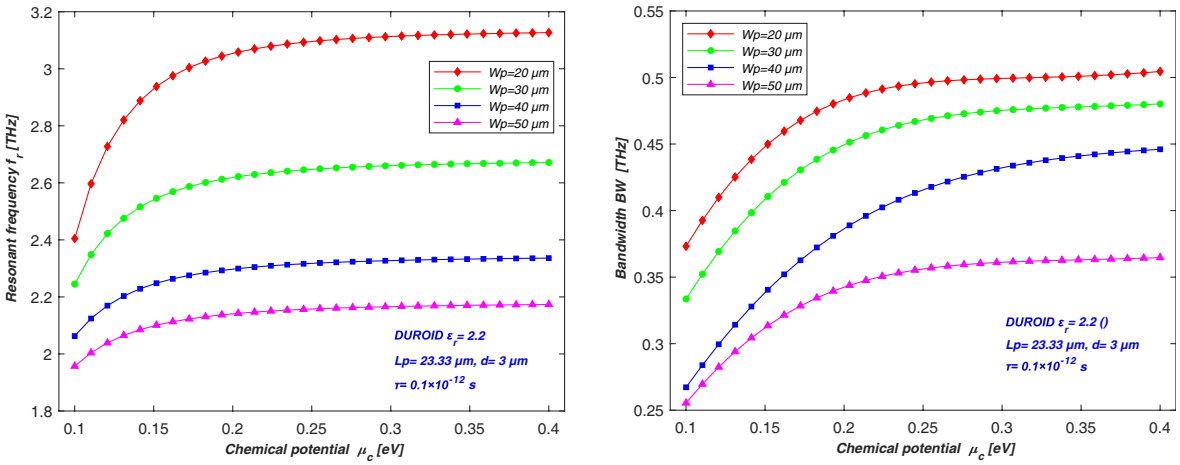

(a) (b)

Figure 6. Resonant frequency and bandwidth versus chemical potential for different values of dielectric constant of substrate.

3.4. Effect of Length of Patch (Lp)

We indicated that the same parameters were used in the previous part, where we fixed the width (Wp) and modified the length (Lp) of the GRMPA structure. In Fig. 7 and Table 5, the dependence of the resonant frequency and bandwidth on the patch length (Lp) is presented. We observe that contrary to the variation of the width of the patch, the resonance frequency and bandwidth increase when the width of patch increases.

Table 5. Resonant frequency and bandwidth versus chemical potential for different values of length of patch.

	μ_c [eV]	$Lp/Wp = 2/3$	$Lp/Wp = 3/4$	$Lp/Wp = 4/5$	$Lp/Wp = 5/6$
FR [THz]	0.1	2.288	2.555	2.651	2.667
	0.2	2.712	2.928	3.113	3.202
	0.3	2.756	2.975	3.179	3.276
	0.4	2.768	2.989	3.200	3.299
BW [THz]	0.1	0.303	0.336	0.373	0.401
	0.2	0.416	0.438	0.461	0.474
	0.3	0.445	0.446	0.467	0.478
	0.4	0.451	0.458	0.477	0.496

Table 6. Resonant frequency and bandwidth versus chemical potential for different values of length of patch.

	μ_c [eV]	$d = 1\,\mu$m	$d = 2\,\mu$m	$d = 3\,\mu$m	$d = 4\,\mu$m
FR [THz]	0.1	2.561	2.499	2.466	2.379
	0.2	3.048	2.887	2.842	2.751
	0.3	3.091	2.934	2.886	2.789
	0.4	3.102	2.947	2.899	2.799
BW [THz]	0.1	0.331	0.373	0.414	0.435
	0.2	0.455	0.487	0.512	0.548
	0.3	0.488	0.504	0.519	0.560
	0.4	0.496	0.509	0.530	0.568

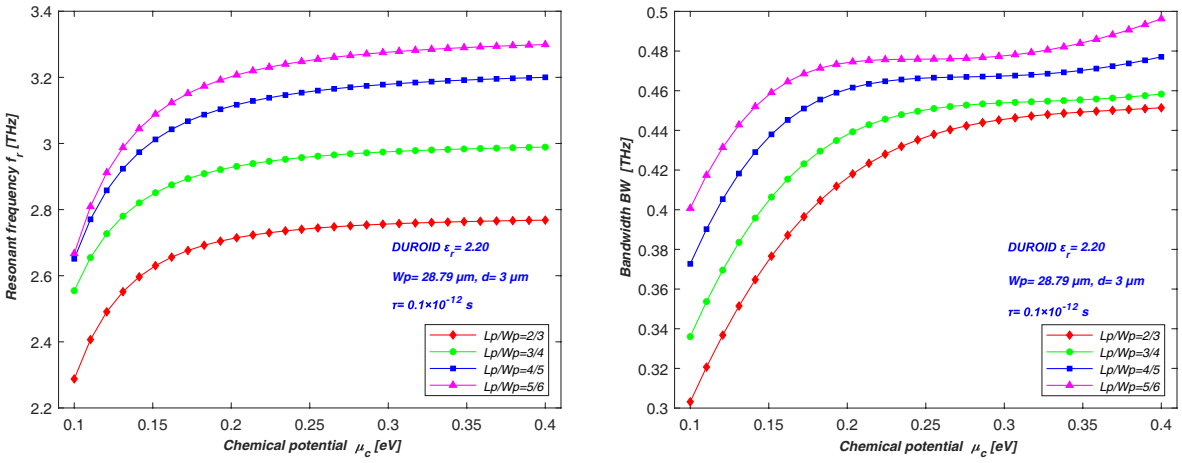

(a) (b)

Figure 7. Resonant frequency and bandwidth versus chemical potential for different values of patch length.

3.5. Effect of Substrate Thickness (d)

In Table 6 and Fig. 8, we investigate the influence of the chemical potential and the thickness of the substrate on the resonant frequency and bandwidth of the GRMPA structure. The rectangular patch

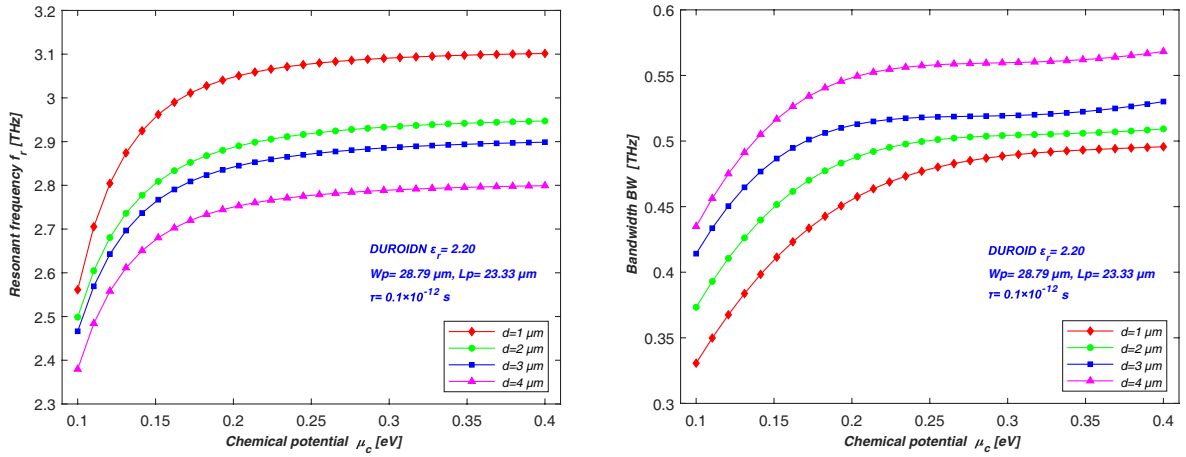

Figure 8. Resonant frequency and bandwidth versus chemical potential for different values of patch length.

of size $Lp = 23.33\,\mu\text{m}$, $Wp = 28.79\,\mu\text{m}$ is made of a thin graphene film with $\tau = 10^{-13}\,\text{s}$. It is observed that the resonant frequency increases with increasing chemical potential for low substrate thicknesses. On the other hand, the bandwidth is very important for very high substrate thickness values.

Table 7 reports our numerical results for the resonant frequency and bandwidth of GRMPA structure isotropic substrate which have been compared with previously simulated published results [9, 34, 35]. It is a very encouraging result of GRMPA structure compared to others rectangular patch antenna bandwidth. This is due to several properties of complex material graphene, and it can be easily integrated and miniaturized.

Table 7. Comparison table of resonant frequency and bandwidth with previous research work.

	Fr [THz]	BW [THz]
Graphene proposed	2.020	0.353
Graphene [9]	2.130	0.325
FR4 [34]	2.45×10^{-3}	2.40×10^{-6}
Arlon [35]	0.693	4.50×10^{-6}

4. CONCLUSION

A spectral domain approach has been used for the numerical calculation of the characteristics of a graphene rectangular microstrip patch antenna (GRMPA). Initially, we use an integral method of moment, which enable us to exploit the spectral tensor of green. The resolution of the integral equations of the electric field leads to a system of homogenous equations. We have calculated the frequency of resonance complexes of antenna. The obtained results show that the resonance frequency of antenna varies significantly with the chemical potential (μ_c) and relaxation time (τ) of conductivity of graphene, which are found strongly dependent on the permittivity of substrate. The properties of the GRMPA structure were stable at chemical potential higher than 0.35 eV. Also computations show that the dimension of rectangular patch can be adjusted to have the maximum operating frequency of the GRMPA structure. On the other hand, the bandwidth increases monotonically with increasing the substrate thickness. The calculated results have been compared with simulated ones available in the literature, and excellent agreement has been found.

REFERENCES

1. Keshavarz, S., A. Abdipour, A. Mohammadi, and R. Keshavarz, "Design and implementation of low loss and compact microstrip triplexer using CSRR loaded coupled lines," *AEU — International Journal of Electronics and Communications*, Vol. 111, 152913, 2019.
2. Chettah, C., O. Barkat, and A. Chaabi, "Tunable properties of optical selective filters based on one-dimensional plasma superconductor photonic crystal," *Journal of Superconductivity and Novel Magnetism*, Vol. 34, 2239–2248, 2021.
3. Keshavarz, S., R. Keshavarz, and A. Abdipour, "Compact active duplexer based on CSRR and interdigital loaded microstrip coupled lines for LTE application," *Progress In Electromagnetics Research C*, Vol. 109, 27–37, 2021.
4. Llatser, I., C. Kremers, A. Cabellos-Aparicio, J. M. Jornet, E. Alarcón, and D. N. Chigrin, "Graphene-based nano-patch antenna for terahertz radiation," *Photonics and Nanostructures-Fundamentals and Applications*, Vol. 10, No. 4, 353–358, 2012.
5. Wang, R., S. Raju, M. Chan, and L. J. Jiang, "Low frequency behavior of CVD graphene from DC to 40 GHz," *Progress In Electromagnetics Research C*, Vol. 71, 1–7, 2017.
6. Krid, H. B., Z. Houaneb, and H. Zairi, "Reconfigurable graphene annular ring antenna for medical and imaging applications," *Progress In Electromagnetics Research M*, Vol. 89, 53–62, 2020.
7. Khan, M. A. K., T. A. Shaem, and M. A. Alim, "Analysis of graphene based miniaturized terahertz patch antennas for single band and dual band operation," *Optik*, Vol. 194, 163012, 2019.
8. Khan, M. A. K., T. A. Shaem, and M. A. Alim, "Graphene patch antennas with different substrate shapes and materials," *Optik*, Vol. 202, 163700, 2020.
9. Hlali, A., Z. Houaneb, and H. Zairi, "Dual-band reconfigurable graphene-based patch antenna in terahertz band: Design, analysis and modeling using WCIP method," *Progress In Electromagnetics Research C*, Vol. 87, 213–226, 2018.
10. Khan, M., A. Kaium, M. Ullah, R. Kabir, and M. A. Alim, "High-performance graphene patch antenna with superstrate cover for terahertz band application," *Plasmonics*, Vol. 15, No. 6, 1719–1727, 2020.
11. Shubham, A., D. Samantaray, S. K. Ghosh, S. Dwivedi, and S. Bhattacharyya, "Performance improvement of a graphene patch antenna using metasurface for THz applications," *Optik*, 169412, 2022.
12. Temmar, M. N. E., A. Hocini, D. Khedrouche, and T. A. Denidni, "Analysis and design of MIMO indoor communication system using terahertz patch antenna based on photonic crystal with graphene," *Photonics and Nanostructures-Fundamentals and Applications*, Vol. 43, 100867, 2021.
13. Gatte, M. T., P. J. Soh, H. A. Rahim, R. B. Ahmad, and F. Malek, "The performance improvement of THz antenna via modeling and characterization of doped graphene," *Progress In Electromagnetics Research M*, Vol. 49, 21–31, 2016.
14. Kiani, N., F. T. Hamedani, and P. Rezaei, "Realization of polarization adjusting in reconfigurable graphene-based microstrip antenna by adding leaf-shaped patch," *Micro and Nanostructures*, 207322, 2022.
15. Song, R., C. Wang, Q. Chen, and D. He, "High conductivity graphene based films for antenna application," *IEEE International Conference on Microwave and Millimeter Wave Technology (ICMMT)*, 1–3, 2020.
16. Vashi, R., T. Upadhyaya, and A. Desai, "Graphene-based wide band semi-flexible array antenna with parasitic patch for smart wireless devices," *International Journal of Microwave and Wireless Technologies*, Vol. 14, No. 1, 86–94, 2022.
17. Dhariwal, S., V. K. Lamba, and A. Kumar, "Simulation and performance analysis of carbon nano-materials based patch antennas," *Indian Journal of Science and Technology*, Vol. 9, No. 4, 1–8, 2016.

18. Blackledge, J. M., A. Boretti, L. Rosa, and S. Castelletto, "Fractal graphene patch antennas and the THz communications revolution," *IOP Conference Series: Materials Science and Engineering*, 012001, IOP Publishing, 2021.
19. Chopra, K., S. Misra, S. H. Gupta, and A. Rajawat, "Design and optimization of multiarray antenna operating in terahertz (THz) band for in-vivo nanonetworks," *Optik*, 169475, 2022.
20. George, J. N. and M. G. Madhan, "Analysis of single band and dual band graphene based patch antenna for terahertz region," *Physica E: Low-dimensional Systems and Nanostructures*, Vol. 94, 126–131, 2017.
21. Pierantoni, L., D. Mencarelli, M. Bozzi, R. Moro, and S. Bellucci, "Graphene-based electronically tuneable microstrip attenuator," *Nanomaterials and Nanotechnology*, Vol. 4, 18, 2014.
22. Kumar, V., "24 GHz graphene patch antenna array," *The Applied Computational Electromagnetics Society Journal (ACES)*, 676–683, 2019.
23. Aldrigo, M., M. Dragoman, S. Iordanescu, F. Nastase, D. Vasilache, and A. Ziaei, "Gain tunability of graphene patch antennas for the ISM band at 24 GHz," *IEEE International Workshop on Antenna Technology (iWAT)*, 1–4, 2020.
24. Cao, Y. S., L. J. Jiang, and A. E. Ruehli, "An equivalent circuit model for graphene-based terahertz antenna using the PEEC method," *IEEE Transactions on Antennas and Propagation*, Vol. 64, No. 4, 1385–1393, 2016.
25. Zhang, B., J. Zhang, C. Liu, Z. P. Wu, and D. He, "Equivalent resonant circuit modeling of a graphene-based bowtie antenna," *Electronics*, Vol. 7, No. 11, 285, 2018.
26. Di Ruscio, D., P. Burghignoli, P. Baccarelli, D. Comite, and A. Galli, "Spectral method of moments for planar structures with azimuthal symmetry," *IEEE Transactions on Antennas and Propagation*, Vol. 62, No. 4, 2317–2322, 2014.
27. Zargano, G. F., A. M. Lerer, and A. O. Pelevin, "Spectral method for calculation of slotted antennas with layered insulator," *Journal of Communications Technology and Electronics*, Vol. 67, No 1, 17–25, 2022.
28. Barkat, O., "Improving the performances of triangular microstrip antenna with multilayered configuration," *COMPEL: The International Journal for Computation and Mathematics in Electrical and Electronic Engineering*, Vol. 33, No. 1/2, 337–354, 2014.
29. Barkat, O., "Modeling and optimization of radiation characteristics of triangular superconducting microstrip antenna array," *Journal of Computational Electronics*, Vol. 13, No. 3, 657–665, 2014.
30. Park, S. O., C. A. Balanis, and C. R. Birtcher, "Analytical evaluation of the asymptotic impedance matrix of a grounded dielectric slab with roof top functionsvol," *IEEE Transactions on Antennas and Propagation*, Vol. 46, No. 2, 251–259, 1998.
31. Hlali, A., Z. Houaneb, and H. Zairi, "Tunable filter based on hybrid metal-graphene structures over an ultrawide terahertz band using an improved Wave Concept Iterative Process method," *Optik*, Vol. 181, 423–431, 2019.
32. Hanson, G. W., "Fundamental transmitting properties of carbon nanotube antennas," *IEEE Transactions on Antennas and Propagation*, Vol. 53, No. 11, 3426–3435, 2005.
33. Hanson, G. W., "Dyadic Green's functions and guided surface waves for a surface conductivity model of graphene," *Journal of Applied Physics*, Vol. 103, No. 6, 064302, 2008.
34. Hossain, M. B., M. S. Hossain, M. M. Hossain, and M. D. Haque, "Optimization of the feeding point location of rectangular microstrip patch antenna," *Adv. Sci. Technol. Eng. Syst.*, Vol 5, 382–386, 2020.
35. Younssi, M., A. Jaoujal, M. D. Yaccoub, A. El Moussaoui, and N. Aknin, "Study of a microstrip antenna with and without superstrate for terahertz frequency," *Int. J. Innov. Appl. Stud.*, Vol. 2, 369–371, 2013.